# WD60/FAP163 is a dynein intermediate chain required for retrograde intraflagellar transport in cilia

Ramila S. Patel-King[a,*], Renée M. Gilberti[a,*,†], Erik F. Y. Hom[b], and Stephen M. King[a]
[a]Department of Molecular, Microbial and Structural Biology, University of Connecticut Health Center, Farmington, CT 06030; [b]Department of Molecular and Cellular Biology, Harvard University, Cambridge, MA 02138

**ABSTRACT** **Retrograde intraflagellar transport (IFT) is required for assembly of cilia. We identify a *Chlamydomonas* flagellar protein (flagellar-associated protein 163 [FAP163]) as being closely related to the D1bIC(FAP133) intermediate chain (IC) of the dynein that powers this movement. Biochemical analysis revealed that FAP163 is present in the flagellar matrix and is actively trafficked by IFT. Furthermore, FAP163 copurified with D1bIC(FAP133) and the LC8 dynein light chain, indicating that it is an integral component of the retrograde IFT dynein. To assess the functional role of FAP163, we generated an RNA interference knockdown of the orthologous protein (WD60) in planaria. The *Smed-wd60(RNAi)* animals had a severe ciliary assembly defect that dramatically compromised whole-organism motility. Most cilia were present as short stubs that had accumulated large quantities of IFT particle–like material between the doublet microtubules and the membrane. The few remaining approximately full-length cilia had a chaotic beat with a frequency reduced from 24 to ~10 Hz. Thus WD60/FAP163 is a dynein IC that is absolutely required for retrograde IFT and ciliary assembly.**

**Monitoring Editor**
Erika Holzbaur
University of Pennsylvania

Received: May 20, 2013
Revised: Jun 26, 2013
Accepted: Jul 2, 2013

## INTRODUCTION

Intraflagellar transport (IFT) is a complex bidirectional motility system that is required for the assembly and maintenance of both motile and primary/sensory cilia (Rosenbaum and Witman, 2002). In general, the components of this system have been broadly conserved from protists to vertebrates, and defects impact a wide array of motility, signaling, and sensory functions. In vertebrates, this leads to many different developmental defects and complex syndromes (e.g., Pazour *et al.*, 2000; Li *et al.*, 2004; Hildebrandt *et al.*, 2011).

The core of the IFT system consists of particles (or trains) comprising multiple copies of two subcomplexes (termed A and B), which have very distinct protein compositions (Cole, 2003). A combination of genetics, biochemistry, and fluorescence imaging suggests that IFT-B is necessary for anterograde transport, whereas IFT-A functions in the retrograde direction (reviewed in Cole, 2009). Cargoes required for assembly and maintenance of cilia are thought to be loaded onto the IFT trains at the basal body region of the cell. After gated entry into the ciliary compartment, these IFT particles are then transported toward the ciliary tip by one or more kinesin motors (Snow *et al.*, 2004). After reorganization at the tip, IFT particles are returned to the ciliary base by a dynein that is more closely related to canonical cytoplasmic dynein than it is to those that power the axoneme. Mutants defective in known components of this retrograde motor are able only to assemble short ciliary stubs in which the region between the doublet microtubules and the membrane is swollen due to the accumulation of IFT particles that are sent into the organelle but cannot be returned to the cell body (Pazour *et al.*, 1999; Signor *et al.*, 1999).

Two different kinesins have been implicated in anterograde IFT in several organisms (Pan *et al.*, 2006; Wickstead and Gull, 2006), but it has been generally assumed that there is a single dynein holoenzyme responsible for retrograde transport (here termed the IFT dynein for clarity, although it may have additional functions outside of cilia). There has been a suggestion, however, that two different dyneins might participate in this process in *Caenorhabditis elegans* (Hao *et al.*, 2011). In *Chlamydomonas*, the IFT dynein is believed to contain two heavy chain (HC) motor units (D1bHC, encoded at

This article was published online ahead of print in MBoC in Press (http://www.molbiolcell.org/cgi/doi/10.1091/mbc.E13-05-0266) on July 17, 2013.

*These authors contributed equally.

†Present address: Center for Academic Programs, University of Connecticut, Storrs, CT 06269.

Address correspondence to: Stephen M. King (king@neuron.uchc.edu).

Abbreviations used: EM, electron microscopy; FAP, flagellar-associated protein; HC, heavy chain; IC, intermediate chain; IFT, intraflagellar transport; LC, light chain; LIC, light intermediate chain; MBP, maltose-binding protein.

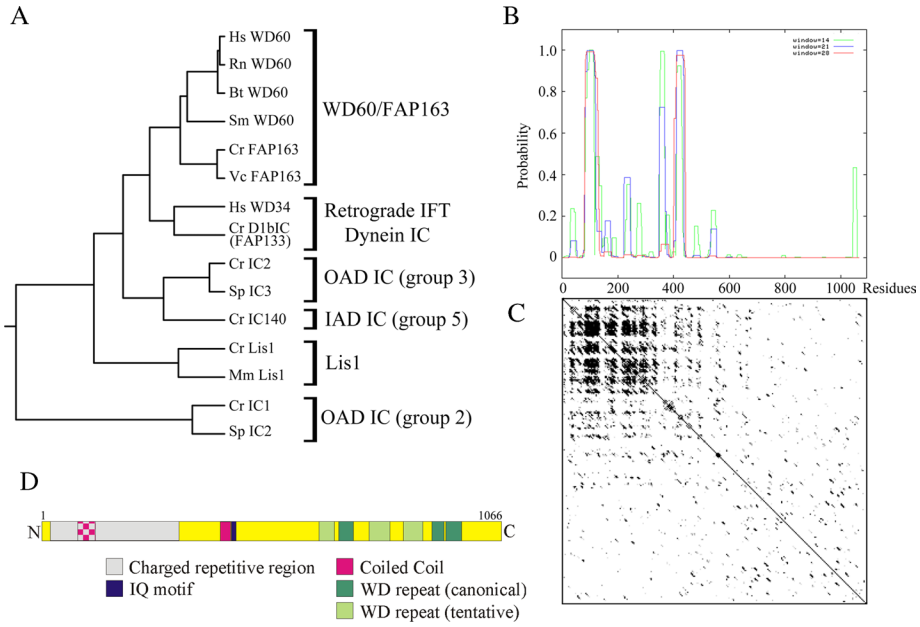


FIGURE 1: Phylogeny and domain organization of WD60/FAP163. (A) The sequences of dynein-associated WD-repeat components, as well as mammalian, planarian, and algal WD60/FAP163 proteins, were aligned using CLUSTALW, and a neighbor-joining tree was generated. All WD60/FAP163 sequences cluster together and are most closely related to the *Chlamydomonas* retrograde dynein IC D1bIC(FAP133) and its human orthologue (WD34). Sequences used were *H. sapiens* (Hs) WD60 (NP_060521), *Rattus norvegicus* (Rn) WD60 (NP_001178702), *Bos taurus* (Bt) WD60 (XP_001788990), *S. mediterranea* (Sm) WD60 (mk4.000489.09.01), *C. reinhardtii* (Cr) FAP163 (XP_001702532), *Volvox carteri* (Vc) FAP163 (XP_002954132), *H. sapiens* WD34 (AAH01614), *C. reinhardtii* D1bIC/FAP133 (BC133909), *C. reinhardtii* IC2 (P27766), *Strongylocentrotus purpuratus* (Sp) IC3 (XP_796667), *C. reinhardtii* IC140 (EDP01123), *C. reinhardtii* Lis1 (ABG33844), *Mus musculus* (Mm) Lis1 (NP_038653), *C. reinhardtii* IC1 (Q39578), and *St. purpuratus* IC2 (XP_003724308). (B) The propensity for coiled-coil formation within human WD60 was analyzed using the COILS algorithm. Two segments have a very high prediction for coiled-coil formation. (C) Comparison of human WD60 against itself using DOTLET (matrix = BLOSUM62; window = 15) revealed that the N-terminal region is repetitive, consisting of multiple charged segments with high similarity. (D) Domain organization of human WD60. The N-terminal region contains two coiled-coil segments embedded within a region predicted to be almost entirely α-helical. The C-terminal domain consists of a series of predicted β-strands; three canonical WD repeats were identified within this region using SMART (residues 686–725, 901–938, and 941–983). WD repeats are often highly degenerate and difficult to identify; visual inspection of the predicted secondary structure, however, suggests that there may be two additional, poorly conserved repeats between the first and second canonical WD repeats and a third before the first canonical repeat. An IQ motif is located between residues 432 and 450.

*DHC16*; Pazour *et al.*, 1999; Porter *et al.*, 1999) that are tightly associated with light intermediate chains (D1bLIC, encoded at *DLI1*; Perrone *et al.*, 2003) and an intermediate chain/light chain (IC/LC) complex that consists of a WD-repeat IC (D1bIC(flagellar-associated protein 133 [FAP133]), encoded at *DIC5*; Rompolas *et al.*, 2007) and the LC8 dynein light chain dimer (encoded at *DLL1*, also known as *FLA14*; Pazour *et al.*, 1998). Canonical cytoplasmic dynein also contains LC dimers of the DYNLT (Tctex1) and DYNLRB (roadblock) families; although these have not yet been identified biochemically within the *Chlamydomonas* IFT dynein (Witman, 2012), there is evidence that a DYNLT orthologue may be part of this complex in *Ca. elegans* (Efimenko *et al.*, 2005). Detailed mechanistic analysis of the IFT dynein has proven rather difficult, as it tends to readily dissociate into at least two different subparticles during purification (Rompolas *et al.*, 2007). One consists of the HC motor and D1bLIC (Pazour *et al.*, 1999; Porter *et al.*, 1999; Perrone *et al.*, 2003), whereas the second contains D1bIC(FAP133) and LC8 (Pazour *et al.*, 1998; Rompolas *et al.*, 2007). It is unclear, however, whether this composition represents the complete particle or whether additional proteins or indeed dynein subtypes are required for retrograde transport.

Here we identify an additional conserved WD-repeat protein that is closely related to D1bIC(FAP133) (the orthologous protein is termed WD34/WDR34 in mammals). This protein (FAP163)[1] is present in the *Chlamydomonas* flagella proteome (Pazour *et al.*, 2005), and its orthologue WD60/WDR60 was upregulated in microarray data for ciliated epithelia in mouse trachea (Hoh *et al.*, 2012), suggesting that it may be involved in IFT. We demonstrate here that *Chlamydomonas* FAP163 is present in the flagellar matrix, associates with D1bIC(FAP133), and is actively trafficked by IFT. Furthermore, we obtained an RNA interference (RNAi)–mediated knockdown of WD60 expression in the planarian flatworm *Schmidtea mediterranea* and found that this protein is indeed absolutely required for ciliary assembly and its lack results in the failure of retrograde IFT.

## RESULTS

### Bioinformatics of dynein-associated WD-repeat proteins

Alignment of dynein IC and related WD-repeat protein sequences by the Panther classification algorithm (PTHR12442) identified a flagellar-associated *Chlamydomonas* WD-repeat protein of unknown function (FAP163; Pazour *et al.*, 2005) as being most closely related to D1bIC(FAP133), which we previously demonstrated was an IC of the dynein complex responsible for retrograde IFT in *Chlamydomonas* (Rompolas *et al.*, 2007). Further analysis using BLAST searches and multiple sequence alignments revealed orthologues of FAP163 (termed WD60/WDR60 in *Homo sapiens*) in a broad range of organisms that assemble cilia, including mammals and other vertebrates, sea urchins, various protists, and the planarian *S. mediterranea* (mk4.000489.09.01; Ψ-BLAST score with human WD60 after two iterations, $9 \times 10^{-103}$; Figure 1A). Sequence analysis of human WD60 (1066 residues; molecular weight, 122,570 Da; pI = 6.88) revealed that it consists of an N-terminal segment that is predicted to be almost completely α-helical, containing two short stretches that have a very high probability of forming coiled coils (Figure 1B) and a repetitive region (residues 24–328) containing many charged residues (Figure 1C), followed by a C-terminal region that is predicted to consist entirely of a series of β-strands with a single short helical segment near the very terminus. Three canonical WD repeats were found within this β-strand segment using the SMART algorithm (Figure 1D). At least three additional putative

[1]As we demonstrate that FAP163 is a dynein IC involved in retrograde IFT, we propose that the *Chlamydomonas* gene name be reassigned as *DIC6* in accordance with the unified nomenclature for ciliary dyneins (Hom *et al.*, 2011). Previously the FAP133 protein was assigned as D1bIC (Hom *et al.*, 2011). Because it is now clear that this dynein contains two different ICs, we suggest that FAP163 and FAP133 be renamed as D1bIC1 and D1bIC2, respectively.

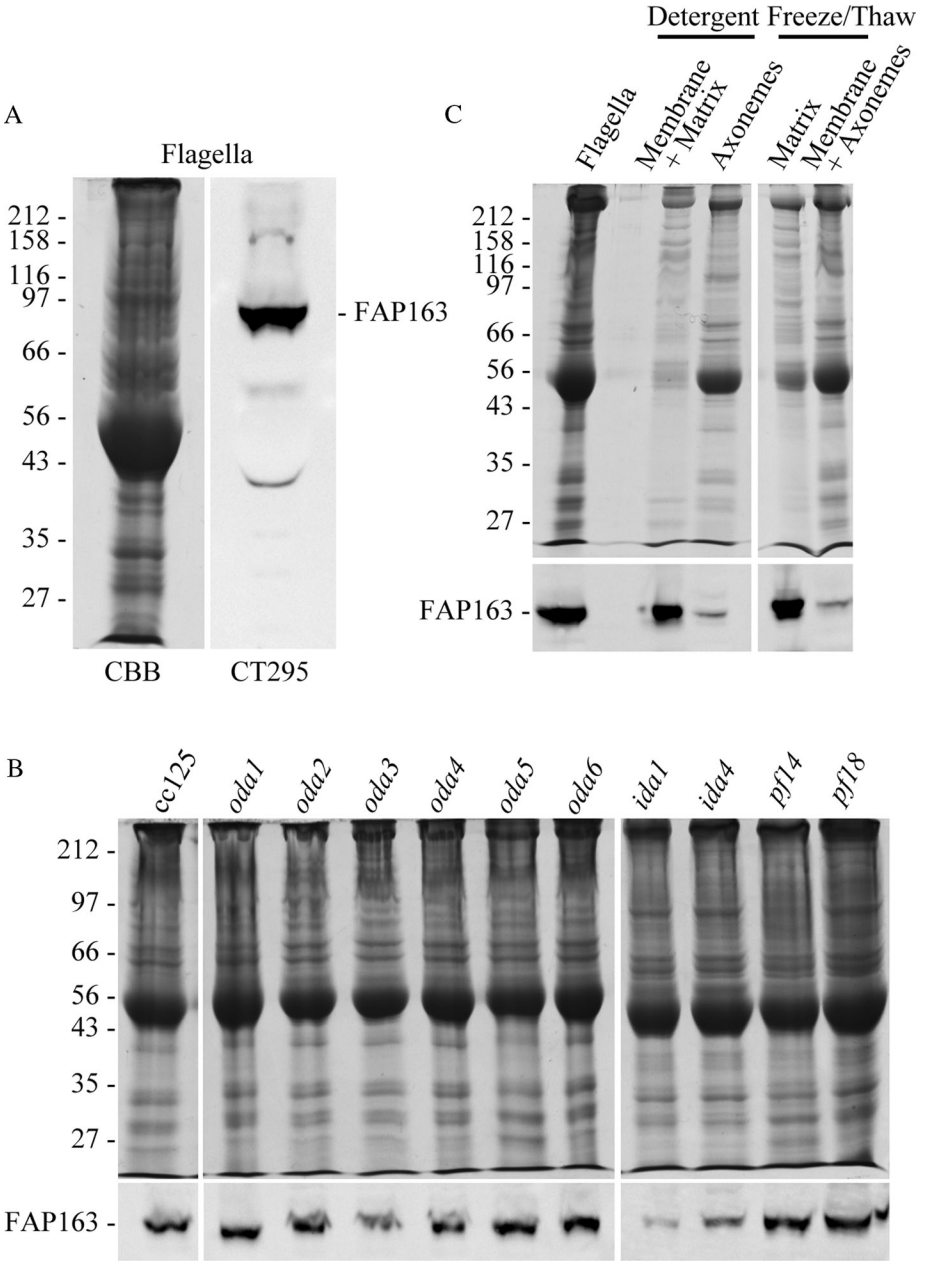


FIGURE 2: FAP163 is a component of the flagellar matrix. (A) Flagellar proteins from the *oda1* mutant were separated in a 10% polyacrylamide gel and either stained with Coomassie blue (CBB) or blotted to nitrocellulose and probed with the CT295 antibody raised against FAP163. The antibody detects a single major band of $M_r$ 89,000 and three very minor bands. (B) Flagella from wild-type *Chlamydomonas* (cc125) and mutants lacking outer arms (*oda1*-*oda6*), inner arms (*ida1* and *ida4*), radial spokes (*pf14*), or the central pair microtubule complex (*pf18*) were electrophoresed in 10% polyacrylamide gels and either stained with Coomassie blue (top) or blotted and probed with CT295 to detect FAP163 (bottom). This protein was present in all the mutant flagella tested. (C) To determine whether FAP163 is associated with the axoneme or part of the flagella matrix, wild-type flagella were extracted with detergent (1% Igepal CA-630) to yield a supernatant containing the membrane and matrix components and a pellet containing the microtubular axoneme. Flagella were also fractionated by three rounds of freeze/thaw, which releases the matrix components but leaves the membrane associated with the axoneme. Top, Coomassie blue-stained 10% polyacrylamide gels; bottom, blots probed with CT295. This reveals that FAP163 is released by both detergent and freeze/thaw, indicating that it is a component of the flagella matrix.

degenerate WD repeats were tentatively identified by visual inspection of the predicted secondary structure; one is located before the first canonical WD repeat and two more as the first and second canonical repeats. In addition, a single IQ motif (residues 432–450) was identified by the Eukaryotic Linear Motif Resource (http://elm.eu.org), suggesting that this protein may bind calmodulin.

### Biochemical analysis of FAP163 in *Chlamydomonas* flagella

Analysis of the *Chlamydomonas* flagellar proteome revealed the presence of FAP163 migrating at $M_r \approx 90{,}000$ (Pazour *et al.*, 2005), although the calculated mass is only 76,134 Da. When blot-purified antibody CT295 raised against the FAP163 C-terminal domain was used to probe samples of wild-type flagella, a single major band of $M_r$ 89,000 was detected, which is completely consistent with the electrophoretic migration of FAP163 observed in the proteomic study (Figure 2A). FAP163 was present in flagella from mutants that lack outer arms (*oda1-6*), inner arms (*ida1*, *ida4*), radial spokes (*pf14*), or the central pair microtubule complex (*pf18*) (Figure 2B), although levels did appear reduced in *ida1* and possibly *ida4*. To determine where FAP163 is located within the flagellum, we solubilized membrane/matrix components by detergent treatment. FAP163 was observed almost exclusively in the soluble fraction. Similarly, most FAP163 was also present in the extract obtained from flagella after multiple rounds of freeze/thaw, which release the flagellar matrix but leave the membrane associated with the axoneme (Figure 2C). Thus FAP163 is a component of the flagellar matrix and is not tightly bound to the microtubular axoneme or the membrane.

To assess the oligomeric state of FAP163, we fractionated freeze/thaw extracts by chromatography in a Superose 6 gel filtration column. FAP163 eluted in a single broad peak with an estimated mass of >350 kDa and precisely copurified with one peak of the LC8 dynein light chain, which is present in multiple flagellar complexes (Figure 3A). Furthermore, we observed that under these solution conditions, FAP163 also coeluted with D1bIC(FAP133), suggesting that both WD-repeat proteins might be part of the same complex. To further test this putative association, we fractionated a wild-type freeze/thaw flagella extract by ion exchange chromatography in a Mono Q column (Figure 3B). D1bIC(FAP133) was found in two distinct peaks, as described previously (Rompolas *et al.*, 2007). We also observed that FAP163 precisely copurified with both D1bIC(FAP133) peaks. These data strongly suggest that FAP163 and D1bIC(FAP133) are associated within the same IC/LC complex

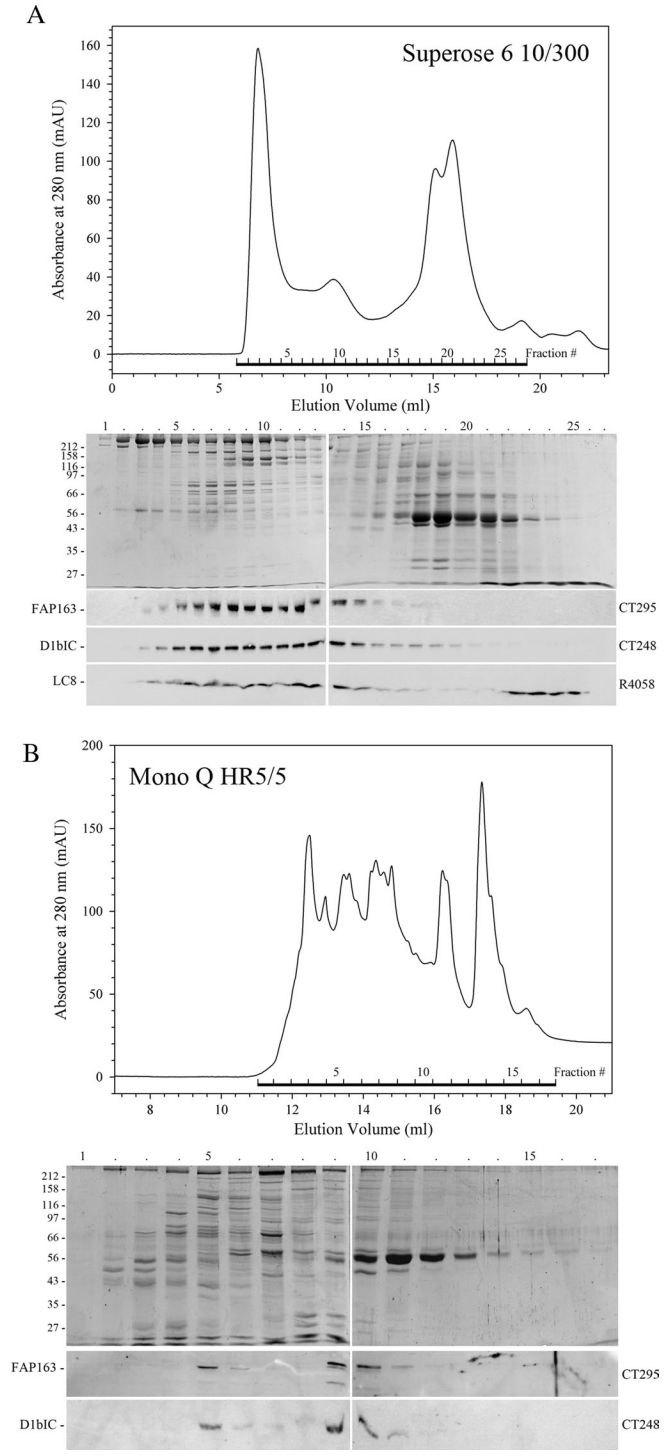


FIGURE 3: FAP163 and D1bIC(FAP133) associate with each other and the LC8 dynein light chain. (A) Chromatogram of an *oda1* freeze/thaw extract fractionated by gel filtration in a Superose 6 10/300 column. The bar indicates the region analyzed by SDS–PAGE. Bottom, these fractions were separated in 10% polyacrylamide gels and stained with Coomassie blue or blotted and probed with CT295, CT248, and R4058 to reveal FAP163, D1bIC(FAP133), and LC8, respectively; samples for analysis of LC8 content were separated in 12.5% gels. (B) Chromatogram of a wild-type (cc125) freeze/thaw extract applied to a Mono Q anion exchange column and eluted with a 0–1 M gradient of NaCl. Top, the resulting chromatogram, bottom, immunoblots corresponding to the region on the chromatogram indicated by the bar. D1bIC(FAP133) and FAP163 coelute in two separate peaks.

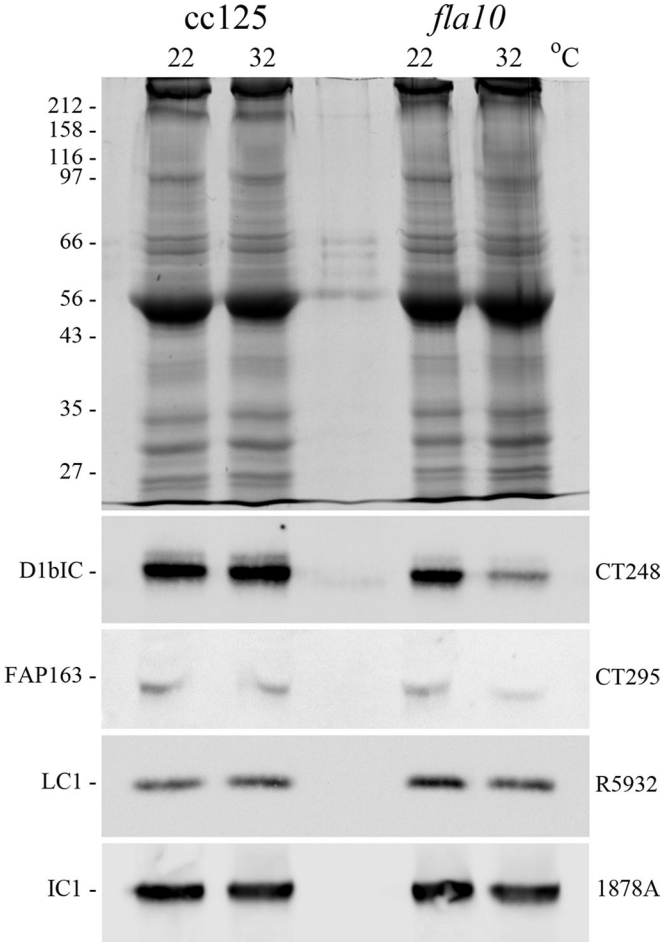


FIGURE 4: FAP163 is trafficked by the intraflagellar transport machinery. Wild-type (cc125) and *fla10* cells were maintained for 3 h at either the permissive (22°C) or restrictive (32°C) temperature. Flagella were isolated and then electrophoresed in 10 or 12.5% polyacrylamide gels. Top, Coomassie blue-stained 10% gel; bottom, immunoblots probed with antibodies CT248, CT295, R5932, and 1878A to detect D1bIC(FAP133), FAP163, LC1, and IC1, respectively. Both D1bIC and FAP163 levels were reduced in *fla10* flagella at the restrictive temperature, suggesting that they are actively trafficked by the IFT machinery, whereas LC1 and IC1 are not.

To determine whether FAP163 is transported by the IFT machinery, we incubated wild-type (cc125) and *fla10* cells at 22 or 32°C for 3 h and then deflagellated them. As expected, analysis of the resulting flagella revealed that D1bIC(FAP133), a component of the retrograde IFT motor, was highly depleted in flagella from *fla10* cells held at the restrictive temperature compared with wild type. Similarly, FAP163 levels also were reduced, whereas those of the axoneme-associated outer arm dynein proteins LC1 and IC1 were not (Figure 4). This result indicates that flagellar FAP163 is actively trafficked by IFT.

### RNAi-mediated knockdown of WD60 in planaria

No *Chlamydomonas* FAP163 mutant currently exists. Therefore, to test the hypothesis that WD60/FAP163 might represent another dynein IC that plays a key role in retrograde IFT, we performed an RNAi-mediated knockdown in the planarian *S. mediterranea*. Of interest, this organism lacks a recognizable D1bIC(FAP133). Accordingly, we obtained a 325–base pair region of the WD60 coding region by PCR from planarian first-strand cDNA and subcloned this into the L4440 vector that has opposing T7 promoters and

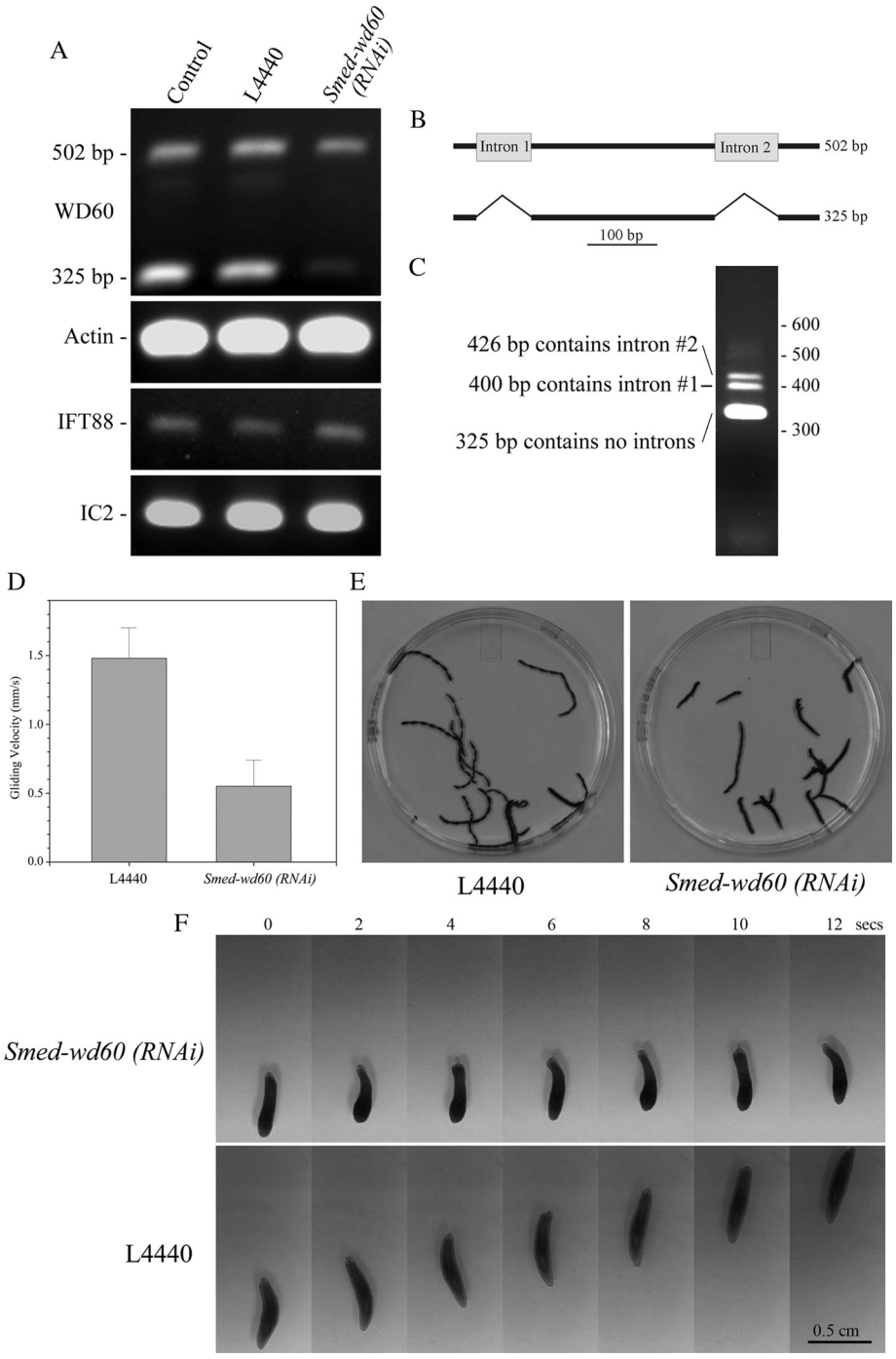


FIGURE 5: *Smed-wd60(RNAi)* planaria exhibit reduced gliding velocity and an altered mode of locomotion. (A) RT-PCR analysis of mRNA levels in untreated control planaria and in animals fed either with the empty L4440 vector or dsRNA from the *Smed-wd60(RNAi)* construct. The first-strand cDNA was prepared using a random hexamer as primer, and the reaction was continued for 25 cycles. Planaria fed with the WD60 dsRNA have unchanged levels of mRNAs encoding actin, IFT88, and outer-arm dynein IC2. Two RT-PCR products (325 and 502 base pairs), however, were detected for WD60. Sequence analysis revealed that both encoded the same region of WD60, but that the larger one also contained two unspliced introns. Levels of the 325–base pair product were greatly reduced in planaria fed with WD60 dsRNA, whereas levels of the 502–base pair product were unchanged. The 502–base pair product was not obtained following treatment of the RNA sample with DNaseI before PCR (not shown), indicating that it derives from genomic DNA. (B) Map of the two RT-PCR products for WD60 shown in A, indicating the location of the two introns. (C) Products obtained by RT-PCR after 40 cycles following DNaseI treatment of the mRNA sample and first-strand cDNA synthesis using an oligo-dT primer. The two additional products derive from partially spliced polyadenylated mRNA for WD60. (D) Bar chart illustrating the velocity of movement of control and *Smed-wd60(RNAi)* planaria. The controls moved by cilia-driven gliding at a rate of 1.48 ± 0.21 mm/s (mean ± SD; $n = 7$), whereas the knockdown animals used waves of muscle contraction and traveled at 0.55 ± 0.19 mm/s ($n = 13$). (E) The tracks taken by individual planaria over a 30-s period. These images were prepared from the decompiled videos by overlaying every 100th frame using Photoshop (and see Supplemental Movie S1). (F) Mode of planarian movement. Controls move with a smooth, cilia-driven gliding motion, whereas *Smed-wd60(RNAi)* animals use peristaltic waves of muscle contraction. These images were taken from the decompiled combined video (see Supplemental Movie S2).

expressed double-stranded RNA (dsRNA) in *Escherichia coli* strain HT115(DE3). Planaria were fed every 2–3 d for several weeks with this dsRNA or with bacteria containing an empty vector.

Analysis of mRNA by RT (reverse transcription)-PCR from first-strand cDNA prepared using a random hexamer as the primer revealed that two bands for WD60 were present. One product obtained was the originally targeted 325–base pair fragment that encodes the central portion of the WD60 protein, whereas the second product of 502 base pairs consisted of this same exonic segment but included two unspliced introns (Figure 5, A and B). The 502–base pair product was not observed when first-strand cDNA was prepared using oligo-dT as the primer for reverse transcriptase, nor was it obtained when the original RNA sample was treated with DNaseI. Consequently, this second product derives from genomic DNA. Of interest, when first-strand cDNA was prepared using an oligo-dT primer, we obtained the 325–base pair product and two minor additional products that included one or the other of the two introns (Figure 5C). Thus planaria maintain a detectable pool of partially spliced polyadenylated mRNA for WD60. RT-PCR using total RNA derived from *Smed-wd60(RNAi)* planaria further revealed that ingestion of WD60 dsRNA resulted in greatly decreased amounts of the 325–base pair product compared with empty vector or no vector controls but had essentially no effect on transcript levels for actin, IFT88, or IC2 (Figure 5A).

### Phenotypic analysis of *Smed-wd60(RNAi)* planaria

We next monitored organismal gliding locomotion and found that *Smed-wd60(RNAi)* animals moved at 0.55 ± 0.19 mm/s (mean ± SD; $n = 13$) compared with 1.48 ± 0.21 mm/s ($n = 7$) for empty vector controls (Figure 5, D and E, and Supplemental Movie S1). This

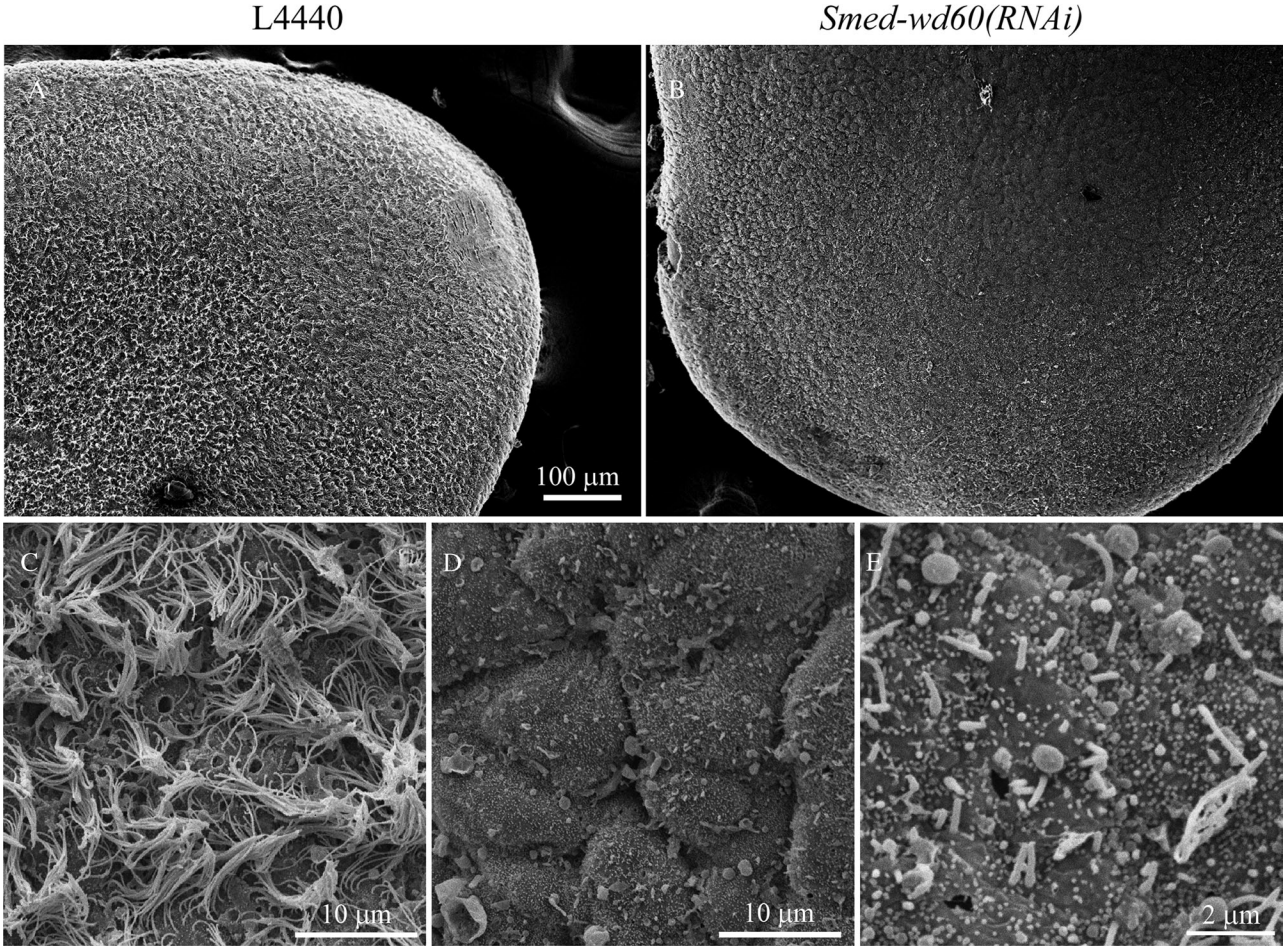


FIGURE 6: *Smed-wd60(RNAi)* planaria have defects in ciliary assembly. Scanning electron micrographs of the ventral surface of control (L4440; A, C) and *Smed-wd60(RNAi)* (B, D, E) animals. The control planaria have many closely apposed cilia that are ~10 µm in length. In contrast, the ventral surface of *Smed-wd60(RNAi)* animals have large areas that are almost devoid of full-length cilia but instead have many ciliary stubs that are <0.5 µm long. Bars,100 µm (A, B), 10 µm (C, D), and 2 µm (E).

decrease in gliding velocity is similar to that observed for planaria that lack functional outer dynein arms (*Smed-ic2(RNAi)*) or indeed are unable to assemble cilia at all (*Smed-ift88(RNAi)*; Rompolas *et al.*, 2010). Furthermore, *Smed-wd60(RNAi)* animals exhibited the alteration in the mode of motility, from cilia-driven gliding to peristaltic waves of muscular contraction, that was found previously (Rompolas *et al.*, 2010) to be a defining characteristic of defects in ciliary assembly and motility (Figure 5F and Supplemental Movie S2). After prolonged feeding with dsRNA for >4 wk, *Smed-wd60(RNAi)* planaria became essentially stationary and had no discernible cilia at the dorsal/ventral margin when examined by differential interference contrast microscopy. Furthermore, these planaria were unable to use the musculature in the rear of the body and eventually split approximately halfway along their length, leading to the partial disintegration of the animal.

Examination of the ventral surface by scanning electron microscopy (EM) of animals fed the RNAi vector for ~3 wk revealed a dramatic reduction in both number and length of cilia assembled by *Smed-wd60(RNAi)* planaria compared with controls (Figure 6). In control animals, the ventral epithelium bore thousands of ~10-µm-long cilia, especially toward the anterior and in the central region surrounding the pharyngeal pore (Figure 6, A and C). In contrast, only relatively few almost-full-length cilia and many short ciliary stubs (<0.5 µm in length) were evident on *Smed-wd60(RNAi)* planaria (Figure 6, B, D, and E). These observations suggested that WD60 is required for ciliary assembly. To further assess this hypothesis, we examined cilia and ciliary stubs from *Smed-wd60(RNAi)* planaria by thin-section transmission EM (Figure 7). We found that the ciliary stubs contained doublet microtubules and associated structures but had an enlarged diameter due to the presence of large quantities of amorphous electron-dense material located between the axonemal doublet microtubules and the ciliary membrane. Indeed, even in longer cilia, accumulations of this material were readily evident.

High-speed video microscopy and kymograph analysis revealed that the few longer cilia remaining on the ventral surface of *Smed-wd60(RNAi)* planaria were motile (Figure 8A and Supplemental Movie S3). Their beat appeared uncoordinated, however, and occurred at rates of ~10–14 Hz; some cilia were observed to protrude essentially vertically from the epithelium and to move only at the base, leading to a twitching motion. In contrast, the cilia of control animals exhibited a high degree of metachronal synchrony and beat at ~24 Hz with both power and recovery strokes (Figure 8B and Supplemental Movie S4).

## DISCUSSION

In this article we examine the functional role of WD60/FAP163, a WD-repeat protein that has been broadly conserved among ciliated organisms. Sequence analysis suggests that this protein is an IC of

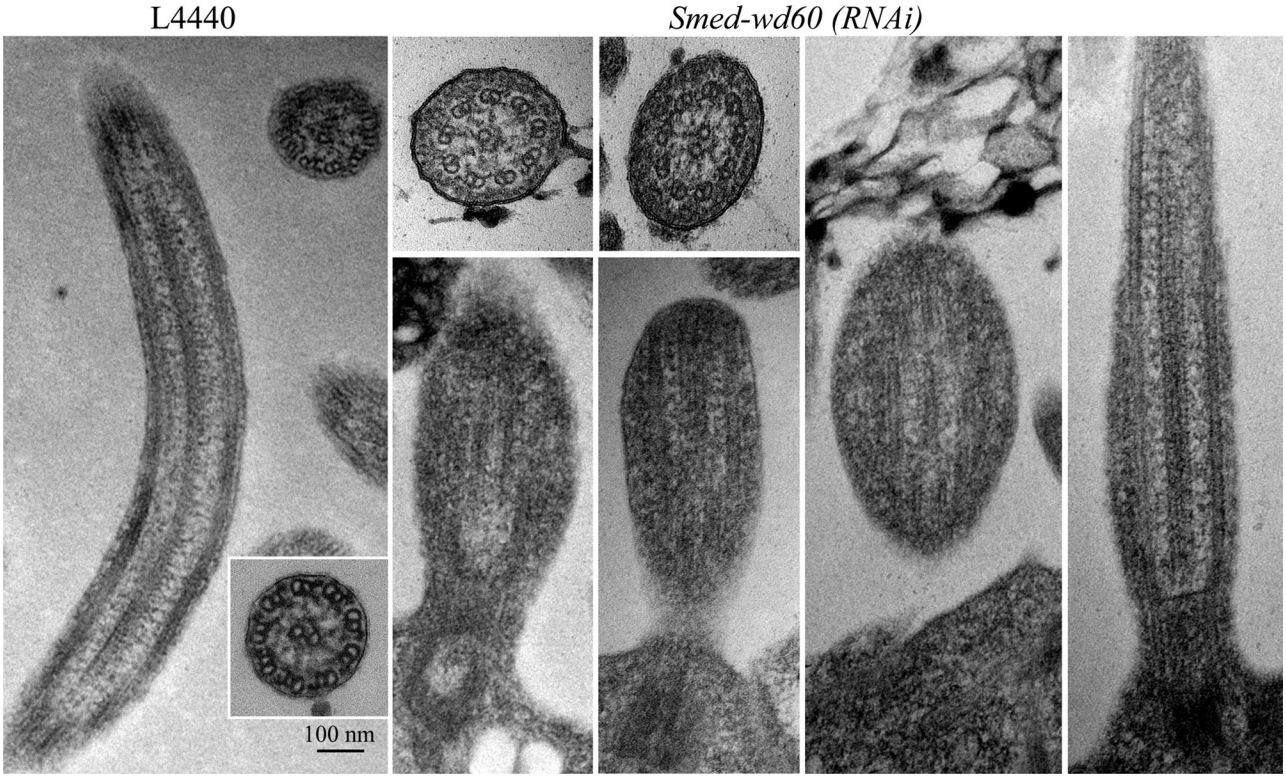


FIGURE 7: Cilia and ciliary stubs present on *Smed-wd60(RNAi)* planaria contain large quantities of IFT particles. Transmission electron micrographs of cilia on the ventral surface of control animals (L4440; left) and cilia and ciliary stubs of *Smed-wd60(RNAi)* planaria (right). The accumulation of electron-dense material (presumably IFT particles) between the doublet microtubules and ciliary membrane is clearly evident in both longitudinal and transverse sections of the knockdown animals; in contrast, this accumulated material is absent from control cilia. Bars, 100 nm.

the dynein that powers retrograde intraflagellar transport, and we find that it is indeed present in the *Chlamydomonas* flagellar matrix and actively trafficked by the IFT machinery. Disruption of WD60/FAP163 function in planaria by RNAi results in failure of ciliary assembly and accumulation of IFT particle-like material in the resulting ciliary stubs, with consequent disruption of organismal motility. Previously an essentially identical ciliary assembly phenotype in *Chlamydomonas* was demonstrated to be caused by the failure of retrograde IFT dynein function (Pazour *et al.*, 1999; Porter *et al.*, 1999). Thus it appears that WD60/FAP163 is an integral dynein IC that in planaria is absolutely required for ciliary assembly.

### FAP163/WD60 is a component of the IFT machinery and required for retrograde IFT

Phylogenetic analysis reveals that WD60/FAP163 groups with the dynein IC subfamily of WD-repeat proteins, and indeed these proteins are most closely related to D1bIC(FAP133 or WD34), which we previously demonstrated to be part of the IFT dynein in *Chlamydomonas* (Rompolas *et al.*, 2007). Mammalian WD60 has an N-terminal region that is highly repetitive and contains two segments of coiled coil followed by a C-terminal domain consisting of WD-repeat motifs. Furthermore, there is a single IQ motif located within the N-terminal region. Although this motif does not appear to be present in *Chlamydomonas* FAP163, it does raise the possibility that WD60 in vertebrates binds calmodulin and thus may be responsive to alterations in $Ca^{2+}$ levels. In contrast, D1bIC(FAP133) consists of a short N-terminal domain containing two degenerate LC8 binding sites followed by a C-terminal segment consisting of six WD repeats (Rompolas *et al.*, 2007).

Biochemical analysis reveals that FAP163 is almost exclusively present in the flagellar matrix, as are core IFT components and associated kinesin and dynein motors. Using the *fla10* temperature-sensitive anterograde IFT mutant, we found that FAP163 was reduced in *Chlamydomonas* flagella when cells were held at the restrictive temperature, suggesting that this protein is indeed trafficked by IFT. In contrast, the flagellar levels of FAP163 were not affected by the presence or absence of outer arms, radial spokes, or the central pair complex, although they did appear decreased in the *ida1* and perhaps also *ida4* inner-arm dynein mutants. When expression of WD60/FAP163 was disrupted in planaria, we observed severe disruption of ciliary structures such that, in general, only short ciliary stubs were retained. These stubs contained accumulated material located between the outer doublet microtubules and the membrane, as is commonly seen in *Chlamydomonas* strains unable to undergo retrograde IFT (Pazour *et al.*, 1998, 1999; Porter *et al.*, 1999). Thus WD60/FAP163 is absolutely required for retrograde IFT. This failure of ciliary assembly on the ventral epithelium led to a change in planarian whole-organism locomotion from cilia-driven gliding to muscle-based peristaltic waves, which we demonstrated previously is characteristic of defects in ciliary assembly or motile behavior (Rompolas *et al.*, 2010).

### Organization of the dynein motor that powers retrograde intraflagellar transport

Dyneins with multiple HC motor units (outer arm, inner-arm I1/f, and canonical cytoplasmic dynein) all contain an IC/LC complex that at a minimum consists of two WD-repeat ICs associated with dimers of three distinct LC species and is absolutely required for assembly of

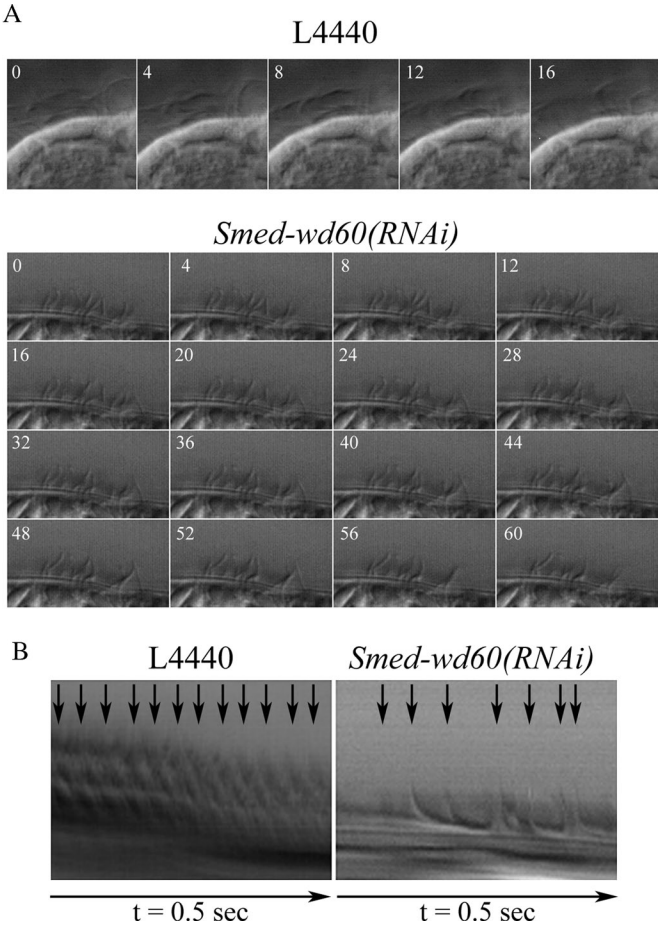


FIGURE 8: Cilia assembled by *Smed-wd60(RNAi)* planaria have an aberrant beat. (A) Sequential frames from the decompiled videos taken at 250 fps of ciliary beating for control and *Smed-wd60(RNAi)* planaria. The numbers at top left in each frame indicate the time in milliseconds. Cilia in the knockdown animals are capable of motility, although their beat is uncoordinated and chaotic. In some cases, the cilia twitch from the base and do not show evidence of effective power and effective strokes (see Supplemental Movies S3 and S4). (B) Kymographs (0.5 s) illustrating the beat frequency of control and *Smed-wd60(RNAi)* planaria. The arrows indicate each beat cycle.

the dynein particle (Tang *et al.*, 1982; Mitchell and Kang, 1991). The ICs within these complexes associate directly (Mitchell and Rosenbaum, 1986; King *et al.*, 1991; Lo *et al.*, 2006), whereas LC binding apparently brings structure to inherently disordered regions of the ICs (Nyarko *et al.*, 2004). In axonemal dyneins, the two ICs in the complex are different gene products and form obligate heterodimers (reviewed in King, 2012), whereas in canonical mammalian cytoplasmic dynein the various alternative spliced forms of the two very closely related IC genes are capable of forming both homodimers and heterodimers (Lo *et al.*, 2006), although whether all of the possible combinations actually occur in vivo is uncertain.

Previously the dynein that powers retrograde IFT in *Chlamydomonas* was known to contain a distinct HC and associated light IC (LIC), as well as D1bIC (also known as FAP133 or WD34) with bound LC8 dimer. Our biochemical analysis using two different chromatographic procedures to fractionate *Chlamydomonas* flagellar matrix components demonstrated that FAP163 is also part of this complex, and thus FAP163 and D1bIC(FAP133) presumably form a heterodimer that is further stabilized by LC8. The similar reductions in flagellar levels of both FAP163 and D1bIC(FAP133) in the *fla10* mutant shifted to the restrictive temperature further supports this suggestion. We also observed that FAP163 and D1bIC(FAP133) elute together in two distinct complexes after anion exchange, and we demonstrated previously that both these peaks of D1bIC(FAP133) subsequently migrate at ~7 S in sucrose density gradients (Rompolas *et al.*, 2007) and are thus not associated with the D1bHC. This raises the possibility that there are two forms of the IC/LC complex. Further biochemical analysis will be required to determine whether these two IC/LC complex forms differ in protein content or whether the change in elution properties is the result of posttranslational modifications.

Intriguingly, although platyhelminths such as *Ca. elegans* and *S. mediterranea* express most components of the IFT dynein and exhibit retrograde IFT (e.g., Signor *et al.*, 1999), they do not encode a recognizable orthologue of D1bIC (Wickstead and Gull, 2012). Given that ICs are believed to be essential for the assembly and function of dyneins with multiple motor domains, this observation was rather puzzling, as it implied that the dynein mediating retrograde IFT in platyhelminths might have an organization distinct from that of all other multimotor dyneins. Our present results suggest an alternative; namely, that some organisms (such as *Chlamydomonas* and vertebrates) actually employ two distinct dynein ICs for retrograde IFT, whereas planarians appear to have secondarily lost the orthologue of D1bIC(/FAP133/WD34) and only use WD60/FAP163. Thus in *Schmidtea* the IC/LC complex of the IFT dynein may be composed of a FAP163/WD60 homodimer; alternatively, it is possible that an additional IC awaits identification in this organism. Surprisingly, *Ca. elegans* also appears to lack a WD60/FAP163 orthologue; thus there may be even more diversity in IFT dynein components. Indeed, it has been reported that a second IFT dynein based on a different HC may exist in *Ca. elegans* (Hao *et al.*, 2011), further suggesting that the mechanisms of retrograde IFT are more complex than originally envisaged.

### Retrograde IFT and human ciliopathies

Defects in the HC that powers retrograde IFT (DYNC2H1) have been demonstrated to cause ciliopathies in humans and have been particularly associated with short-rib polydactyly and asphyxiating thoracic dystrophy (Jeune's syndrome; Dagoneau *et al.*, 2009; Merrill *et al.*, 2009). Furthermore, HC mutations that result in premature termination occur only in the heterozygous state, suggesting that the phenotype is hypomorphic (Schmidts *et al.*, 2013). Mutations in the NEK1 kinase and the core IFT component IFT80 also result in the failure of ciliary assembly and lead to similar phenotypes (Beales *et al.*, 2007; Thiel *et al.*, 2011), although DYNC2H1 mutations are considered to be the major cause (Baujat *et al.*, 2013). Our demonstration that lack of the WD60/FAP163 IFT dynein IC results in a severe ciliary assembly defect in planaria due to the failure of retrograde IFT thus raises the clear possibility that in vertebrates, mutations in this gene might cause phenotypes similar to those observed for DYNC2H1, NEK1, and IFT80. Indeed, a very recent report indicates that point mutations that result in truncation of WDR60 before the WD-repeat domain lead to both short-rib polydactyly and Jeune's syndrome (McInerney-Leo *et al.*, 2013).

## MATERIALS AND METHODS

### Bioinformatics

*Chlamydomonas* FAP163 was classified as a close relative of D1bIC/FAP133 (WD34 in vertebrates) by the Protein Analysis Through Evolutionary Relationships (PANTHER) clustering algorithm (www.pantherdb.org). Orthologous sequences from other organisms

closely related to *Chlamydomonas* FAP163 were identified using BLAST. Alignments with known dynein-associated WD-repeat proteins were generated using CLUSTALW (www.clustal.org) and the output used to construct a neighbor-joining phylogenetic tree. The secondary structure of WD60 was assessed using PREDICTPROTEIN (www.predictprotein.org). Identification of WD-repeat domains, coiled-coil regions, and the repetitive N-terminal segment was performed using SMART (http://smart.embl-heidelberg.de), COILS (http://embnet.vital-it.ch/software/COILS_form.html), and DOTLET (www.ikp.unibe.ch/dotlet/dotlet.html), respectively. The IQ motif was identified using the Eukaryotic Linear Motif Resource.

### *Chlamydomonas* strains and culture

*Chlamydomonas reinhardtii* wild-type strains cc124/cc125 and mutants *fla10*, *oda1, oda2, oda3, oda4, oda5, oda6, ida1*, *ida4*, *pf14*, and *pf18* were grown in R medium bubbled with 95% air/5% $CO_2$ on 15:9 h light/dark cycle.

### Preparation of α-FAP163 antibody

Sequence encoding the C-terminal 264 residues of FAP163 was obtained by PCR from first-strand cDNA and subcloned into the pMAL-c2 vector across the *Xmn*I/*Xba*I restriction sites, resulting in a C-terminal fusion to maltose-binding protein (MBP). Expression of the MBP fusion protein in *E. coli* BL21(DE3) was induced with 1 mM isopropylthiogalactoside and the protein subsequently purified by chromatography on an amylose affinity column. The purified fusion protein was then used as the immunogen for antibody production in rabbit CT295 (Covance Immunology Services, Denver, PA). Specific antibody was obtained from the resulting immune serum by blot affinity using the FAP163 C-terminal domain after removal of the MBP fusion partner.

Other antibodies used were rabbit polyclonals CT248, R4058, and R5932 against D1bIC(FAP133), LC8, and LC1, respectively (King and Patel-King, 1995; Benashski *et al*., 1999; Rompolas *et al*., 2007), and mouse monoclonal 1878A, which reacts specifically with IC1 (King *et al*., 1985).

### Flagella preparation and biochemical analysis of *Chlamydomonas* FAP163

*Chlamydomonas* strains were deflagellated with dibucaine and flagella purified by standard methods (King, 1995). Flagella (~3 mg/ml) were demembranated with 1% Igepal CA-630 in HMEK buffer (30 mM 4-(2-hydroxyethyl)-1-piperazineethanesulfonic acid, pH 7.5, 5 mM $MgSO_4$, 0.5 mM EDTA, and 25 mM KCl). Alternatively, matrix components were released by three rounds of freeze/thaw as described previously (Rompolas *et al*., 2007). Chromatographic separations were performed using an ÄKTApurifier-10 workstation (GE Healthcare Biosciences, Piscataway, NJ). Flagellar matrix samples were fractionated by gel filtration in a Superose 6 10/300 column equilibrated in HMEK or were applied to a HR5/5 Mono Q ion exchange column equilibrated with 20 mM Tris-Cl, pH 8.0, and then eluted using a 0–1 M NaCl gradient. For the *fla10* temperature-shift experiment, prewarmed sucrose-containing buffers and dibucaine were added to the cell suspensions so that deflagellation occurred at the appropriate temperature. Subsequent flagella purification steps were performed at 4°C. Samples were electrophoresed in 10 or 12.5% SDS–polyacrylamide gels and either stained with Coomassie brilliant blue or transferred to nitrocellulose, stained with reactive brown 10, and subsequently probed with various antibodies (as described), followed by horseradish peroxidase–conjugated secondary antibodies. Chemiluminescence was detected using ECL reagent and a LAS4000 cooled charge-coupled device (CCD) digital imaging system (both from GE Healthcare Biosciences).

### RNAi in planaria

Colonies of the planarian *S. mediterranea* were maintained and expanded as detailed previously (Rompolas and King, 2009). RNAi was performed essentially as described previously (Newmark *et al*., 2003). In brief, to generate the RNAi construct, a 325–base pair region of the WD60 coding sequence was obtained from first-strand cDNA by PCR and then subcloned across the *Xba*I/*Xho*I sites in plasmid L4440, which contains opposing T7 promoters. dsRNA production was induced after transformation into *E. coli* strain HT115(DE3), which lacks RNase III and thus cannot degrade dsRNA. Bacteria containing dsRNA or the empty vector control were fed to groups of planaria every 2–3 d for several weeks. The mRNA levels of the target and control genes were assessed by RT-PCR using standard methods.

### Video microscopy

Videos of planarian movement in 9-cm Petri dishes were taken with a CCD color camera (DFK 31BU03; The Imaging Source, Charlotte, NC) using IC-capture, version 2.2, software at 30 fps and decompiled using Blaze Media Pro (Mystik Media, Hampstead, NC). Images illustrating the paths taken by individual animals were constructed by overlaying every 100th frame from the decompiled video using Photoshop CS4 (Adobe, San Jose, CA). The 20× real-time movie illustrating this motion was generated by decimating the video frames by 20 while keeping the frame rate at 30 fps using VirtualDub (www.virtualdub.org/). Individual movies were then cropped, combined, and labeled using ImageJ (National Institutes of Health, Bethesda, MD). Higher-magnification real-time videos were taken using a Canon PowerShot SD880 (Canon, Melville, NY), converted with Super C, and processed, cropped, and combined with VirtualDub and ImageJ.

To visualize ciliary beating, individual planaria were confined on a microscope slide by Parafilm spacers or held immobile using a Commodore Compressor (VU e-innovations, Nashville, TN). Cilia at the anterior dorsal–ventral junction were imaged using an Olympus BX51 microscope (Tokyo, Japan) equipped with differential interference contrast optics and either a Plan Apo 60×/1.40 numerical aperture (NA) or 100×/1.35 NA oil objective lens. Videos of ciliary motility were captured using an X-PRI F1 digital camera (AOS Technologies, Baden Daetwil, Switzerland) at 250 fps. The video frame rate, compression, cropping, and brightness/contrast were adjusted using VirtualDub and ImageJ. Videos were decompiled with Blaze Media Pro.

### Scanning and transmission electron microscopy

For scanning EM, planaria were treated overnight with relaxant solution (1% $HNO_3$, 0.85% formaldehyde, 50 mM $MgSO_4$), rinsed with buffer, and then fixed with 2.5% glutaraldehyde in 50 mM Na cacodylate, pH 7.4. Subsequently, samples were postfixed with 1% $OsO_4$ and dehydrated through an ethanol series. After critical-point drying, planaria were mounted, sputter coated with gold, and imaged in a JSM5900 scanning EM (JEOL, Peabody, MA).

To visualize internal ciliary structure, the anterior region of individual planarians was excised and fixed with 1% glutaraldehyde in phosphate-buffered saline for 15 min and then with 1% glutaraldehyde in 50 mM Na cacodylate for 1 h. The fixative solution was changed every 10–15 min to avoid it becoming exhausted due to the large quantity of mucus on the planarian ventral surface. Samples were postfixed with 1% $OsO_4$, stained en bloc with 1% methanolic

uranyl acetate, dehydrated through ethanol, and embedded in Epon. Thin sections were poststained with uranyl acetate and lead citrate and imaged using a Hitachi H-7650 transmission EM (Hitachi, Tokyo, Japan) operating at 80 kV.


## ACKNOWLEDGMENTS

We thank Panteleimon Rompolas (Yale University School of Medicine, New Haven, CT) for many helpful discussions and Maya Yankova (University of Connecticut Health Center, Farmington, CT) for her assistance with electron microscopy. We are also grateful to Carol Wicking (University of Queensland, Brisbane, Australia) for providing a preprint describing human WDR60 mutations before publication. This study was supported by Grant GM051293 from the National Institutes of Health (to S.M.K). E.F.Y.H. was supported in part by the Jane Coffin Childs Memorial Research Fund and the National Institute of General Medical Sciences Center for Systems Biology (GM068763).


## REFERENCES


Baujat G *et al.* (2013). Asphyxiating thoracic dysplasia: clinical and molecular review of 39 families. J Med Genet 50, 91–98.

Beales PL *et al.* (2007). IFT80, which encodes a conserved intraflagellar transport protein, is mutated in Jeune asphyxiating thoracic dystrophy. Nat Genet 39, 727–729.

Benashski SE, Patel-King RS, King SM (1999). Light chain 1 from the *Chlamydomonas* outer dynein arm is a leucine-rich repeat protein associated with the motor domain of the γ heavy chain. Biochemistry 38, 7253–7264.

Cole D (2009). Intraflagellar transport. In: The *Chlamydomonas* Source Book, Vol. 3: Cell Motility and Behavior, ed. GB Witman, San Diego, CA: Elsevier, 71–113.

Cole DG (2003). The intraflagellar transport machinery of *Chlamydomonas reinhardtii*. Traffic 4, 435–442.

Dagoneau N *et al.* (2009). DYNC2H1 mutations cause asphyxiating thoracic dystrophy and short rib-polydactyly syndrome, type III. Am J Hum Genet 84, 706–711.

Efimenko E, Bubb K, Mak HY, Holzman T, Leroux MR, Ruvkun G, Thomas JH, Swoboda P (2005). Analysis of xbx genes in *C. elegans*. Development 132, 1923–1934.

Hao L, Efimenko E, Swoboda P, Scholey J (2011). The retrograde IFT machinery of *C. elegans* cilia: two IFT dynein complexes? PLoS One e20995.

Hildebrandt F, Benzing T, Katsanis N (2011). Ciliopathies. N Engl J Med 364, 1533–1543.

Hoh R, Stowe TR, Turk E, Stearns S (2012). Transcriptional program of ciliated epithelial cells reveals new cilium and centrosome components and links to human disease. PLoS One 7, e52166.

Hom E *et al.* (2011). A unified taxonomy for ciliary dyneins. Cytoskeleton 68, 555–565.

King SM (1995). Large-scale isolation of *Chlamydomonas* flagella. Methods Cell Biol 47, 9–12.

King SM (2012). Composition and assembly of axonemal dyneins. In: Dyneins: Structure, Biology and Disease, ed. SM King, Waltham, MA: Elsevier, 209–243.

King SM, Otter T, Witman GB (1985). Characterization of monoclonal antibodies against *Chlamydomonas* flagellar dyneins by high-resolution protein blotting. Proc Natl Acad Sci USA 82, 4717–4721.

King SM, Patel-King RS (1995). The $M_{(r)}$ = 8,000 and 11,000 outer arm dynein light chains from *Chlamydomonas* flagella have cytoplasmic homologues. J Biol Chem 270, 11445–11452.

King SM, Wilkerson CG, Witman GB (1991). The $M_r$ 78,000 intermediate chain of *Chlamydomonas* outer arm dynein interacts with alpha-tubulin in situ. J Biol Chem 266, 8401–8407.

Li JB *et al.* (2004). Comparative genomics identifies a flagellar and basal body proteome that includes the BBS5 human disease gene. Cell 117, 541–552.

Lo KW-H, Kan H-M, Pfister KK (2006). Identification of a novel region of the cytoplasmic dynein intermediate chain important for dimerization in the absence of the light chains. J Biol Chem 281, 9552–9559.

McInerney-Leo AM *et al.* (2013). Short-rib polydactyly and Jeune's syndrome are caused by mutations in WDR60. Am J Hum Genet (*in press*), DOI: 10.1016/j.ajhg.2013.06.022.

Merrill AE *et al.* (2009). Ciliary abnormalities due to defects in the retrograde transport protein DYNC2H1 in short-rib polydactyly syndrome. Am J Hum Genet 84, 542–549.

Mitchell DR, Kang Y (1991). Identification of *oda6* as a *Chlamydomonas* dynein mutant by rescue with the wild-type gene. J Cell Biol 113, 835–842.

Mitchell DR, Rosenbaum JL (1986). Protein-protein interactions in the 18S ATPase of *Chlamydomonas* outer dynein arms. Cell Motil Cytoskeleton 6, 510–520.

Newmark P, Reddien P, Cebria F, Sanchez-Alvarado A (2003). Ingestion of bacterially expressed double-stranded RNA inhibits gene expression in planaria. Proc Natl Acad Sci USA 100, 11861–11865.

Nyarko A, Hare M, Hays TS, Barbar E (2004). The intermediate chain of cytoplasmic dynein is partially disordered and gains structure upon binding to light-chain LC8. Biochemistry 43, 15595–15603.

Pan X, Ou G, Civelekoglu-Scholey G, Blacque OE, Endres NF, Tao L, Mogilner A, Leroux MR, Vale RD, Scholey JM (2006). Mechanism of transport of IFT particles in *C. elegans* cilia by the concerted action of kinesin-II and OSM-3 motors. J Cell Biol 174, 1035–1045.

Pazour G, Agrin N, Leszyk J, Witman G (2005). Proteomic analysis of a eukaryotic flagellum. J Cell Biol 170, 103–113.

Pazour GJ, Dickert BL, Vucica Y, Seeley ES, Rosenbaum JL, Witman GB, Cole DG (2000). *Chlamydomonas* IFT88 and its mouse homologue, polycystic kidney disease gene tg737, are required for assembly of cilia and flagella. J Cell Biol 151, 709–718.

Pazour GJ, Dickert BL, Witman GB (1999). The DHC1b (DHC2) isoform of cytoplasmic dynein is required for flagellar assembly. J Cell Biol 144, 473–481.

Pazour GJ, Wilkerson CG, Witman GB (1998). A dynein light chain is essential for the retrograde particle movement of intraflagellar transport (IFT). J Cell Biol 141, 979–992.

Perrone C, Tritschler D, Taulman P, Bower R, Yoder B, Porter M (2003). A novel dynein light intermediate chain colocalizes with the retrograde motor for intraflagellar transport at sites of axoneme assembly in *Chlamydomonas* and mammalian cells. Mol Biol Cell 14, 2041–2056.

Porter ME, Bower R, Knott JA, Byrd P, Dentler W (1999). Cytoplasmic dynein heavy chain 1b is required for flagellar assembly in *Chlamydomonas*. Mol Biol Cell 10, 693–712.

Rompolas P, King SM (2009). *Schmidtea mediterranea*: a model system for analysis of motile cilia. Methods Cell Biol 93, 81–98.

Rompolas P, Patel-King RS, King SM (2010). An outer arm dynein conformational switch is required for metachronal synchrony of motile cilia in planaria. Mol Biol Cell 21, 3669–3679.

Rompolas P, Pedersen L, Patel-King RS, King SM (2007). *Chlamydomonas* FAP133 is a dynein intermediate chain associated with the retrograde intraflagellar transport motor. J Cell Sci 120, 3653–3665.

Rosenbaum JL, Witman GB (2002). Intraflagellar transport. Nat Rev Mol Cell Biol 3, 813–825.

Schmidts M *et al.* (2013). Exome sequencing identifies DYNC2H1 mutations as a common cause of asphyxiating thoracic dystrophy (Jeune syndrome) without major polydactyly, renal or retinal involvement. J Med Genet 50, 309–323.

Signor D, Wedaman KP, Orozco JT, Dwyer ND, Bargmann CI, Rose LS, Scholey JM (1999). Role of a class DHC1b dynein in retrograde transport of IFT motors and IFT raft particles along cilia, but not dendrites, in chemosensory neurons of living *Caenorhabditis elegans*. J Cell Biol 147, 519–530.

Snow JJ, Ou G, Gunnarson AL, Walker MRS, Zhou HM, Brust-Mascher I, Scholey JM (2004). Two anterograde intraflagellar transport motors cooperate to build sensory cilia on *C. elegans* neurons. Nat Cell Biol 6, 1109–1113.

Tang WJ, Bell CW, Sale WS, Gibbons IR (1982). Structure of the dynein-1 outer arm in sea urchin sperm flagella. I. Analysis by separation of subunits. J Biol Chem 257, 508–515.

Thiel C *et al.* (2011). NEK1 mutations cause short-rib polydactyly syndrome type Majewski. Am J Hum Genet 88, 106–114.

Wickstead B, Gull K (2006). A holistic kinesin phylogeny reveals new kinesin families and predicts protein functions. Mol Biol Cell 17, 1734–1743.

Wickstead B, Gull K (2012). Evolutionary biology of dyneins. In: Dyneins: Structure, Biology and Disease, ed. SM King, Waltham, MA: Elsevier, 89–121.

Witman GB (2012). Dynein and intraflagellar transport. In: Dyneins: Structure, Biology and Disease, ed. SM King, Waltham, MA: Elsevier, 395–421.